Iraqi Journal of Veterinary Sciences

www.vetmedmosul.com

Reconstruction of experimentally induced radial bone defect in rabbits by using acellular fish swim bladder and autologous bone marrow clot: Histopathological assessment

N.A. Mahdi and N.H. Mahdi

Department of Veterinary Surgery and Obstetrics, College of Veterinary Medicine, University of Baghdad, Baghdad, Iraq

Article information

Article history:
Received 09 October, 2024
Accepted 06 December, 2024
Published online 01 January, 2025

Keywords:
Segmental bone defect
Fish swim bladder
Bone marrow clot
Bone regeneration
Rabbits

Correspondence:
N.H. Mahdi
nadia.hvet@covm.uobaghdad.iq

Abstract

In the current study, forty-five clinically healthy adult male rabbits, 9-12 months old, weighed 1.5-1.7 kg, were used. The experimental animals were randomly divided into three equal groups of 15. In all animals, segmental defects of 5 mm were induced in the midshaft of the radius. The defects were left without additives in the control group (CG). In the fish swim bladder treated group (FSB group), the created bone defects were wrapped using a previously prepared acellular fish swim bladder (FSB) and sutured around the bone defects. In the fish swim bladder and autologous bone marrow clot-treated group (FSB-BMC group), the defects were wrapped using FSB as described, with a portion of the aspirated 1 ml bone marrow clot filling each bone defect. The bone defects in all groups were evaluated histopathologically at 4,8- and 12-weeks post-operation to observe the bone formation and bridging of segmental bone defects. The results showed a significant increase in osteoblasts, osteocytes, Haversian canals, neovascularization blood vessels, and bone tissue formation in the FSB-BMC treated group compared to other groups at 4 weeks post-operation. At 8- and 12-weeks post-surgery, both treated groups showed a significant increase in osteoblasts, osteocytes, mature bone, bone trabeculae, Haversian canals and bone tissue compared to the control group. In conclusion, the FSB-BMC treated group showed a higher new bone formation and complete bridging than other groups. In contrast, the FSB-treated group showed new bone formation and partial bridging compared to the control group.

DOI: 10.33899/ijvs.2024.154298.3937,

Introduction

Segmental bone defect repair resulting from trauma, infection, bone tumor resection or congenital malformation is still an essential challenge for orthopedic surgeons (1-4). The preferred treatment option for healing bone loss is bone grafting, which is useful in managing delayed union, nonunion, and arthrodesis (5). Clinically, autograft, allograft, and xenograft have been utilized as graft substitutes (6). Autograft is the gold standard for bone grafting (7,8). Critical advances have been conducted in the bone tissue engineering field, with the intent to supplement the utilization of autogenous bone grafts to keep away from the adverse consequences related to them-for instance, cells, biomaterials and growth factors that have improved regenerating bone (9). Extracellular matrix (ECM) derived biomaterials have been clinically used to repair different tissues and organs (10-17). Different types of intact ECM have been utilized as biological scaffolds to encourage the remodeling of organs and tissues; these ECM scaffolds have been commonly gathered from the small intestine, urinary bladder, skin, pancreas, liver, and pericardium (18-21). Fish swim bladder (FSB) collagen, the essential constituent of the ECM, has the advantages of low immunity, significant biocompatibility, and biodegradability. It is easily available, has no cost, and is easily decellularized. It is mainly

composed of collagen I, with low cellularity compared to other tissues with extremely strong mechanical strength because of its inflation function, which is crucial during tissue regeneration (22). Collagen membranes from fish swim bladders are used as a strong and acid-resistant suture for pH regulated stomach perforation and tendon rupture, and research on biomaterials for tissue engineering prepares appropriate scaffolds from FSB use in the application of vascular graft (23,24). Cell-based therapies are considered one of the enhancing methods for tissue healing. The three primary approaches developed and utilized for tissue regeneration are bone marrow aspirate (BMA), bone marrow concentrate, and cultured mesenchymal stem cells (MSCs) (25). For the successful repair of bone, cartilage, and soft tissues, bone marrow aspirate is a great source of endogenous reparative cells and growth factors (26-31). Bone Marrow Aspiration BMA is the direct aspiration of autologous bone marrow from the iliac crest and long bones such as the humerus or femur. BMA tends to coagulate when collected due to the presence of megakaryocytes, platelets, and coagulation factors, and there is a strong reason for using BMA clots for tissue regeneration strategies (32).

This study investigated the effect of acellular fish swim bladder (FSB) alone and with an autologous bone marrow aspirate clot on the healing of radial segmental defects in rabbits.

Materials and methods

Ethical approval

All procedures utilized in the present study received ethical approval from the local committee on animal care and use at the College of Veterinary Medicine, University of Baghdad (No: P.G/1222, June 26th, 2024).

Experimental animals

The current investigation utilized 45 clinically healthy adult rabbits weighing 1.5-1.7 kg and 9-12 months. They were housed in special cages 60*50*50 centimeters metal crates in the College of Veterinary Medicine. Throughout the trial, these animals were maintained at room temperature, 22±3ºC for 15 days to acclimatize before surgery. They were fed green grass and commercial pellets, and all animals were given 0.2 mg/kg. BW (S/C) Ivermectin (AVICO, Jordan) for internal parasites and mange (33).

Experimental design

The 45 experimental animals were divided equally into three groups (n=15); segmental defects measuring 5 mm were induced in each animal's mid-shaft of the radius bone. The defects were left without additives in the control group (CG). In the fish swim bladder treated group (FSB group), the created defects were wrapped using the previously prepared acellular fish swim bladder (FSB) and sutured around the bone defects. In the fish swim bladder and autologous bone marrow clot treated group (FSB-BMC group), the defects were wrapped using FSB as previously described after filling the bone defect with autologous clotted bone marrow. The segmental defects in all groups were evaluated histopathologically at 4, 8 weeks and 12 weeks post-operation to observe the development of new bone formation and complete bridging in the defect site.

Preparation of acellular fish swim bladder (FSB)

Fresh swim bladders of carp fish were obtained from the local market and transported to the lab in a phosphate buffer solution (PBS) container. After removing the outer fat and blood capillaries, the swim bladders were rinsed and washed with PBS at 37ºC for 15 minutes. The FSB scaffolds were decellularized using the chemical decellularization method, which involved lysing the cell membrane and other cellular components with 0.5% sodium dodecyl sulphate (SDS) for 24 hours at room temperature and gently shaking the container three times (34,35). The decellularized scaffolds were cut into approximately 1*1.5 cm pieces and terminally sterilized for 2 hours using 0.1% Peracetic acid (PAA) and 4% ethanol solution (36). Then the scaffolds were washed for 15 minutes at 37ºC using phosphate buffer solution (PBS) and terminally stored in sterile PBS containing streptomycin (100 µg/ml), penicillin (100 IU/ml) and Amphotericin (100 µg/ml) and preserved at 4ºC (34).

Anesthetic protocol

Acepromazine (1 mg/kg) was injected intramuscularly into the experimental animals to sedate them (Prozil Fort, Vietnam). Following 10 minutes duration, an intramuscular combination of 40 mg/kg of 10% Ketamine (Alfasan-Holland) and 5 mg/kg of 2% Xylazine Hydrochloride (VMD-Belgium) was administered as a general anesthesia (37,38).

Bone marrow aspiration

The animal was placed into a lateral recumbency after giving general anesthesia and undergoing routine strict aseptic preparation of the aspiration field. A tiny stab skin incision was made to facilitate entry of the aspiration needle gauge 16 in the mid-way between the head of the femur and the greater trochanter. The location of the trochanter fossa can be determined by palpating the greater trochanter and the needle inserted toward the trochanteric fossa and carefully rotated until the medullary cavity was reached to obtain 1ml of BM sample using a sterile syringe (Figure 1). The aspirated BM was allowed to clot for fifteen minutes before implantation and cut to fit the created radial defect of the same animal (29,39).

Surgical operation

The anesthetized experimental animals were placed in a right lateral recumbency position following aseptic preparation of the right forelimb's surgical site from the

humerus's mid-shift to the metacarpal bones. A 3-4 cm skin incision was performed on the right forelimb's cranio-medial aspect, an equivalent distance between the elbow and carpal joint. (Figure 2A). The pronator teres and flexor carpi radialis muscles were carefully separated with fine blunt scissors to expose the radius bone (Figure 2B). The 5mm distance was marked at the radius midshaft for osteotomy (Figure 2C), the marked segment (5 mm) was removed using electrical saw irrigated using 0.9% sterile saline solution to create a defect in the radius midshaft (Figure 2D). In the control group the segmental bone defect was left empty. In contrast, in the FSB group, the defect was wrapped using the previously prepared acellular FSB and sutured as a tube around the radius bone defect (Figure 2E). In contrast, in the FSB-BMC group, the radial defect was wrapped using acellular FSB and filled with autologous bone marrow clot (Figure 2F). Subsequently, a simple continuous pattern using 5/0 polydioxanone (PDS) was used to suture the FSB membrane (Figure 2G). The muscles were approximated by a simple continuous suture pattern using 3/0 polydioxanone (PDS) and an interrupted suture pattern with 3/0 silk, and the subcutaneous and skin closed routinely (Figure 2H). Intramuscular injection of meloxicam at a dose of 1.5 mg/ kg. B.W. was administered as an analgesic agent (40), and penicillin-streptomycin antibiotics were administered at 10,000 IU/Kg B.W. and 5 mg/Kg B.W. for 3 days post-operation (41).

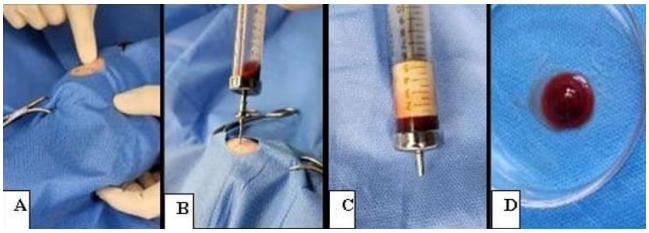

Figure 1: Steps of bone marrow aspiration (A) Palpating the greater trochanter. (B) The aspiration needle is inserted toward the trochanteric fossa. (C) The aspirated BM is left to clot before implantation. (D) Bone marrow clot sample.

Results

Histology of acellular fish swim bladder

The histological sections of fish swim bladder before decellularization showed the muscularis mucosa consisting of a sheet of smooth muscle with cell nuclei and submucosa with dense wavy collagen fiber (Figure 3A). While the histological sections, after decellularization, showed wavy dense staining acellular collagen fiber and loose, delicate light-stained elastic fibers (Figure 3B).

Histology of bone marrow clot

The histological sections of the bone marrow clot showed bone marrow fragments with various cells, such as neutrophils, lymphoid cells, erythroid cells, and megakaryocytes (Figure 4).

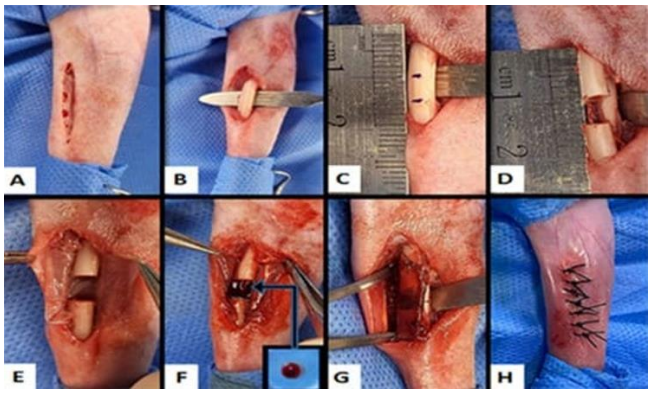

Figure 2: Steps of surgical procedure (A) A 3-4 cm skin incision is performed on the right forelimb's cranio-medial aspect. (B) Expose the radius bone after separating the muscles. (C) 5mm distance at the radius mid shaft is marked for osteotomy. (D) Creation of5mm segmental bone defect. (E) The radial defect is wrapped with acellular FSB. (F) The radial defect is filled with bone marrow clot after wrapping with acellular FSB. (G) The FSB membrane is sutured. (H) Sutured skin.

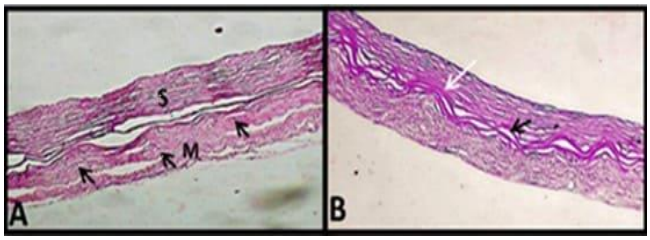

Figure 3: Histological section of FSB scaffold. (A) Before decellularization, shows the muscularis mucosa (M) consist of sheet of smooth muscle with cell nuclei (arrows) and submucosa (S) with dense wavy collagen fibres (B) after decellularization, shows wavy dense staining collagen fiber (black arrow) and loose delicate light-stained elastic fibers (whit arrow) (H&E stain 100X).

At four weeks post-operation

The histopathological sections in the control group showed endochondral bone regeneration at the bone edges containing hypertrophic chondrocytes accompanied by the formation of thin, irregular new bone (woven bone) widely spaced by remnants of mesenchymal tissue and partially lined with immature osteoblasts (Figure 5A). Other observations revealed the newly formed bone tissue, which was widely spaced by vascular fibrous tissue with several chondrocytes and blood vessels. Also, marrow cavities lining with osteoblasts were seen (Figure 5B and C).

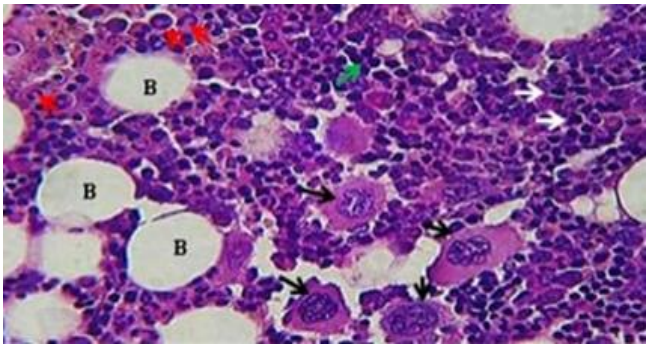

Figure 4: Histological section in Bone marrow clot sample, shows bone marrow fragments (B), with numbers of neutrophil cells (red arrow), lymphoid cells (white arrow), erythroid cells (green arrow) and megakaryocyte (black arrow) (H&E stain 400X).

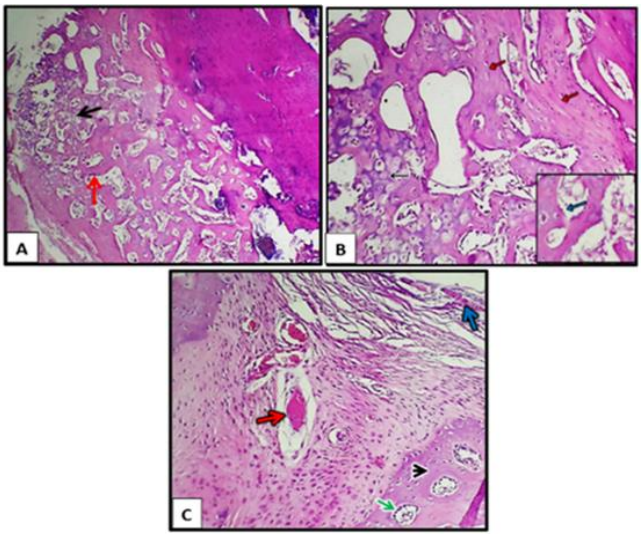

Figure 5: Histopathological section in control group at 4 weeks post operation. (A) shows endochondral bone regeneration at the bone edges containing hypertrophic chondrocyte (black arrow) accompanied by formation of thin irregular new bone (woven bone) widely spaced by remnant of mesenchymal tissue and partially lining with immature osteoblast (red arrow) (H&E stain 100X). (B) shows the newly bone tissue (red arrow) that widely spaced by vascular fibrous tissue with numbers of chondrocyte (black arrow) and osteoblast (blue arrow) (H&E stain 100X & 400X). (C) shows the newly bone tissue (black arrow) with blood vessels (red arrow) and marrow cavities lining with osteoblast (green arrow) and periosteum (blue arrow) (H&E stain 400X).

In the FSB-treated group, the histopathological findings at this period showed thick trabecular bone lining with active osteoblasts with resorbed cavities extended in vascular-rich granulation tissue with active surface osteoblasts attached to the fractured bone, with osteocytes and few newly formed Haversian canals (Figure 6A). Other sections showed increased collagen density in the fibrous tissue that filled the fracture site with newly formed capillaries with the remnant of the FSB scaffold (Figure 6B). Other observations showed thin bone trabeculae that contain osteocytes in lacunae and are entirely lined with active osteoblasts surrounded by rich collagen granulation tissue invaded by mononuclear cells (MNCs) (Figure 6C).

In the FSB-BMC-treated group, the histopathological manifestation showed the presence of new trabeculae with a thick fibrous border associated with highly vascularized stroma (Figure 7A). Other sections showed obvious denes of newly formed bone at highly vascular fibroblast stroma with perivascular MNC infiltration (Figure 7B). Several segments of new bone trabeculae were seen in other sections, with complete osteoblast lining surrounded by a thick zone of fibrous tissue and evidence of a bone marrow clot remnant (Figure 7C).

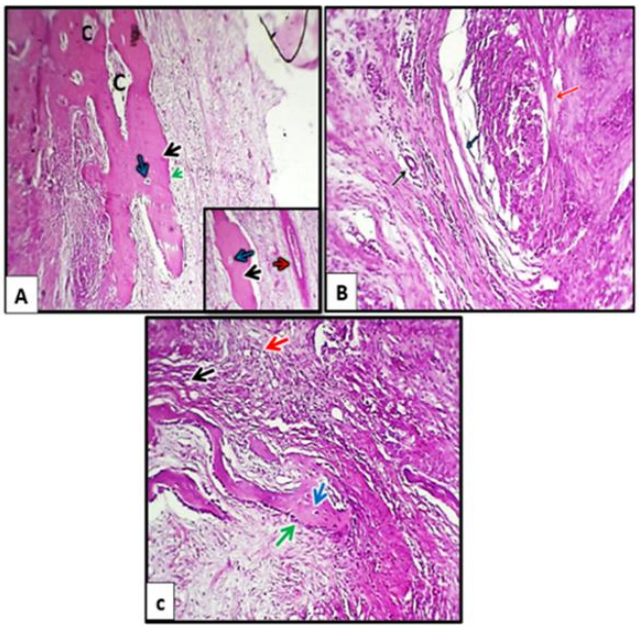

Figure 6: Histopathological section in FSB treated group 4 weeks post-operation. (A) shows thick trabecular bone with few osteocytes (black arrow) lining with active osteoblast (green arrow) with resorbed cavities (C) extended in vascular granulation tissue (red arrow) with few newly formed Haversian canals (blue arrow). (H&E stain 100X & 200X). (B) shows increased collagen density in the fibrous tissue (red arrow) that filled the fracture site with newly formed capillaries (black arrow) with the remnant of FSB scaffold (blue arrow) (H&E stain 200X). (C) shows thin bone trabeculae that contain osteocytes in lacunae (blue arrow) and are completely lined with active osteoblast (green arrow) surrounded by rich collagen granulation tissue invaded by mononuclear cells (MNCs) (red arrow) (H&E stain 200X).

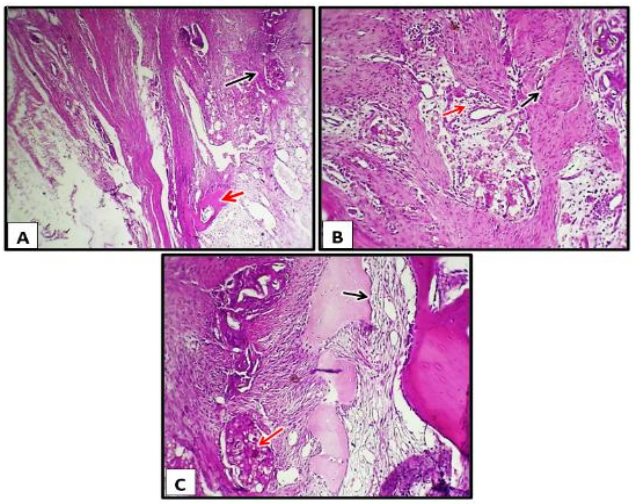

Figure 7: Histopathological section in FSB-BMC treated group at 4 weeks post-operation. (A) It shows the presence of a new trabeculae (red arrow) with a thick fibrous border associated with highly vascularized stroma (black arrow) (H&E stain 100X). (B) It shows a new bone formation (black arrow) at highly vascular fibroblast stroma with prevascular MNCs infiltration (red arrow) (H&E stain 200X). (C) It shows several segments of new bone that are entirely lined with osteoblast (black arrow) and surrounded by a thick zone of fibrous tissue, with evidence of bone marrow clot remnant (red arrow) (H&E stain 200X).

At eight weeks post-operation

The histopathological findings in the control group represent disordered trabeculae of new bone formation bound to the fracture site of the host bone (Figure 8A). Other sections showed fibrocartilaginous tissue extending between newly bone trabeculae attached to the host bone, which showed numerous mature chondrocytes within fibrous tissue (Figure 8B). In the FSB-treated group, the histopathological findings at this period showed the formation of thick lamellar bone with widened Haversian canals attached to the end of the fracture site surrounded by fatty marrow (Figure 9A). Other sections showed several new bone branches attached to the FSB membrane remnant surrounded by fatty marrow (Figure 9B). The main histopathological findings at this period were a moderate increase in osteonal canal formation within calcified cartilage, with high numbers of osteoblasts within osteonal canals surrounded by thick fibrous connective tissue (Figure 9C). In the FSB-BMC-treated group, the histopathological findings at this period revealed complete replacement of the fracture site with thick lamellar bone lined with active osteoblasts and numerous osteocytes and contained wide Haversian canals. The new bone was surrounded by fatty marrow with a remnant clot (Figures 10A and B). Other sections revealed thick fibrous proliferation with multiple MNC aggregations that filled the fracture site and attached it to the host bone (Figure 10C).

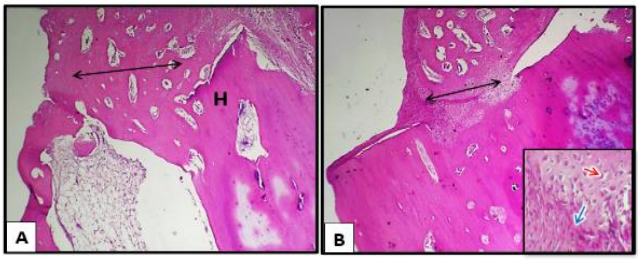

Figure 8: Histopathological section in control group at 8 weeks post operation. (A) Shows disordered trabeculae of new bone formation (black arrow) bound the fracture site of host bone (H) (H&E stain 100X). (B) Shows fibrocartilages tissue extended between newly bone trabeculae (black arrow) attached the host bone that showed numerous mature chondrocyte (red arrow) within fibrous tissue (blue arrow) (H&E stain 100X & 400X).

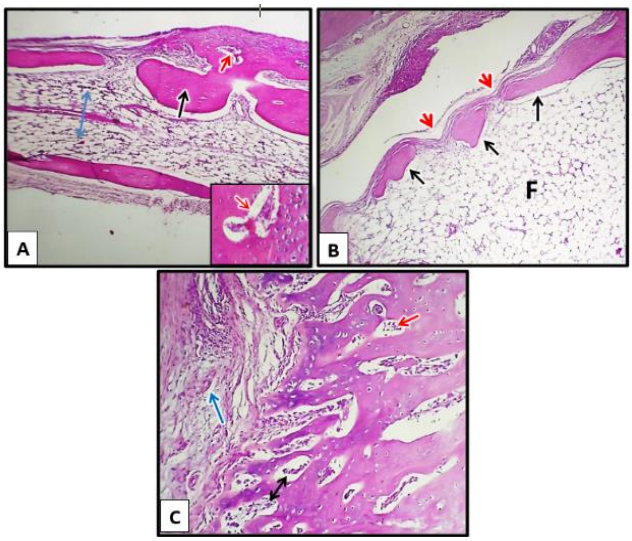

Figure 9: Histopathological section in FSB treated group at 8 weeks post-operation. (A) Shows formation of thick lamellar bone (black arrow) with widened Haversian canal (red arrow) attached to the end of fracture site surrounded by fatty marrow (blue arrow) (H&E stain 100X & 400X). (B) It shows several new bone branches (black arrow) attached to the FSB membrane remnant (red arrow), which is surrounded by fatty marrow (F) (H&E stain 100X). (C) Shows moderate increase of osteonal canal formation (black arrow) within calcified cartilage with high numbers of osteoblast (red arrow) surrounded by thick fibrous connective tissue (blue arrow) (H&E stain 200X).

At twelve-week post operation

In the control group, the histopathological sections showed a moderate amount of lamellar bone formation attached to the old bone with evidence of newly formed small Haversian canals together with the remnant of mesenchymal

tissue, the lamellar bone lining with thin flattened osteoblast with several empty lacunae of osteocyte appeared at the bone edge (Figure 11A and B). Other sections showed irregular delicate trabecular widely spaced by large marrow cavities containing calcified matrix (Figure 11C).

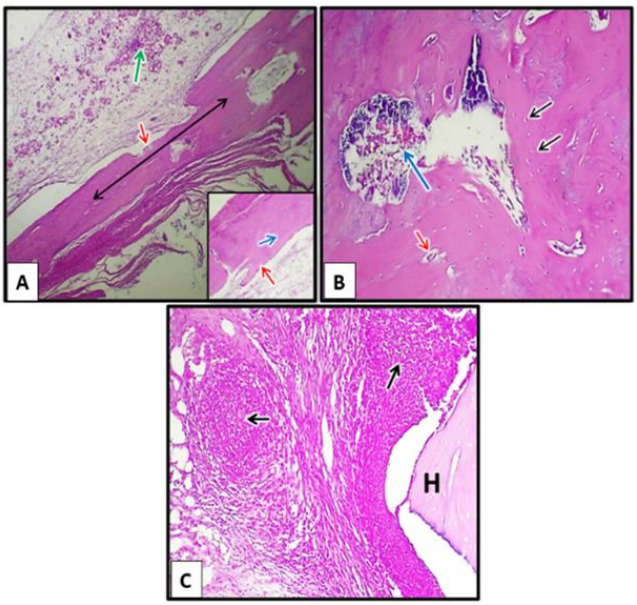

Figure 10: Histopathological section in FSB-BMC treated group at 8 weeks post operation. (A) Shows complete replacement the fracture site with thick lamellar bone (black arrow) complete lining with active osteoblast (red arrow) and numerous osteocytes (blue arrow) and containing wide Haversian canals, the new bone surrounded by fatty marrow with remnant clot (green arrow) (H&E stain 100X). (B) Shows complete replacement the fracture site with thick lamellar bone with numerous osteocytes (black arrow) and containing small Haversian canals (red arrow) with empty cavity filled with debries (blue arrow) (H&E stain 200X). (C) Shows thick fibrous proliferation with multiple MNCs aggregation (black arrow) filled the fracture site and attached to the host bone (H) (H&E stain 200X).

In the FSB-treated group, the histopathological findings at this period showed mature, compact bone with several wide Haversian canals, calcium deposits, and osteocytes (Figures 12A and B). Other sections revealed thick lamellar bone embedded in fatty marrow with elongated osteocytes (Figure 12C). In the FSB-BMC-treated group, the histopathological sections at this period showed the formation of compact bone with small Haversian canals and osteocytes (Figure 13A). Other manifestations showed wide Haversian canals with active osteoblasts and a large resorbed cavity appearance (Figure 13 B and C).

In the present study, the histopathological scores revealed significant differences among groups. There was a significant increase (P≤0.05) in osteoblasts, osteocytes, Haversian canals, new blood vessels and bone tissue formation in the FSB-BMC treated group compared to other groups at 4 weeks post-operation. In contrast, both treated groups revealed a significant increase (P≤0.05) in osteoclast, mature bone, bone trabeculae and inflammation compared to the control group, with no significant differences in granulation tissue formation and bone bridge among groups at this period. At 8 weeks post-surgery, the FSB-BMC treated group showed a significant increase (P≤0.05) in osteoclast, bone bridge and new blood vessels as compared to other groups, while at the same interval, both treated groups showed a significant increase (P≤0.05) in osteoblasts, osteocytes, mature bone, bone trabeculae, Haversian canals and bone tissue as compared to the control group. At 12 weeks post-surgery, both treated groups showed a significant increase (P≤0.05) in osteoblasts, osteocytes, mature bone, bone bridge, Haversian canals and bone tissue as compared to the control group, with no significant differences among groups in the other histopathological index (Table 1).

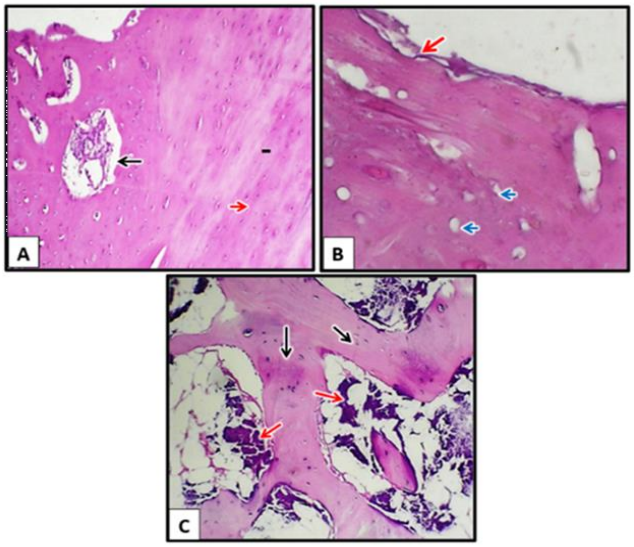

Figure 11: Histopathological section in the control group at 12 weeks post-operation. (A) Shows a moderate amount of lamellar bone formation (L) with numerous newly formed Haversian canals (black arrow) together with a remnant of mesenchymal tissue, with numerous osteocytes (red arrow) (H&E stain 200X). (A) Shows lamellar bone formation lining with thin flattened osteoblast (red arrow) with several empty lacunae of osteocyte appearing at the bone edge (blue arrow) (H&E stain 400X). (C) It shows irregular delicate trabecular bone (black arrows) that are widely spaced by large marrow cavities containing calcified matrix (red arrows) (H&E stain 200X).

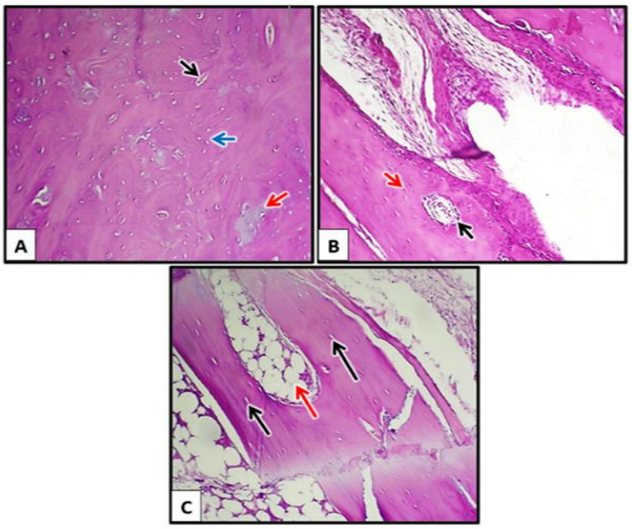

Figure 12: Histopathological section in FSB treated group at 12 weeks post-operation. (A, B) It shows mature compact bone with several small Haversian canals (black arrow), calcium deposits (red arrow), and several osteocytes (blue arrow) (H&E stain 200X). (C) Shows thick lamellar bone with elongated osteocyte (black arrow) embedded in fatty marrow (red arrow) (H&E stain 200X).

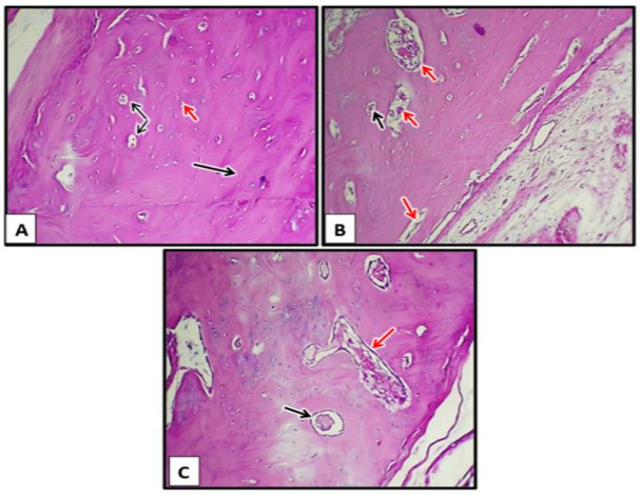

Figure 13: Histopathological section in FSB-BMC treated group at 12 weeks post-operation. (A) Shows the formation of compact bone with numbers of small Haversian canals (black arrow) and osteocytes (red arrow) (H&E stain 200X). (B) It shows compact bone with Haversian canals (black arrow) with numbers of active osteoblasts in addition to large resorbed cavities (red arrows) (H&E stain 100X). (C) Shows wide Haversian canals with numbers of active osteoblast (black arrow) and large resorbed cavity (red arrow) (H&E stain 200X).

Table 1: The mean values of histopathological scores for three groups at different periods

Parameters	4 Week			LSD	8 Week			LSD	12 Week			LSD
	1st	2nd	3rd		1st	2nd	3rd		1st	2nd	3rd	
Osteoblasts	1 c	2 b	3 a	0.77 *	1 b	3 a	3 a	0.82 *	2 b	3 a	3 a	0.88 *
Osteocytes	0 c	2 b	3 a	0.84 *	1 b	3 a	3 a	0.82 *	2 b	3 a	3 a	0.88 *
Osteoclast	0 b	1 a	1 a	0.85 *	0 c	2 b	3 a	0.84 *	0	0	0	0.0 NS
Mature bone	0 b	2 a	2 a	0.92 *	0 b	3 a	3 a	1.07 *	1 b	3 a	3 a	0.82 *
Bone bridge	0	0	0	0.0 NS	0 c	1 b	2 a	0.87 *	0 b	2 a	2 a	0.91 *
Bone trabeculae	1 b	3 a	3 a	0.82 *	2 b	3 a	3 a	0.88 *	2 a	0 b	0 b	0.89 *
HC	0 c	2 b	3 a	0.84 *	0 b	3 a	3 a	1.07 *	0 b	3 a	3 a	1.07 *
Inflammation	1 a	0 b	0 b	0.77 *	1 a	0 b	0 b	0.77 *	1	1	1	0.0 NS
GT	0	0	0	0.0 NS	1 a	0 b	0 b	0.77 *	1	1	1	0.0 NS
New BV	0 c	2 b	3 a	0.84 *	0 c	1 b	3 a	0.98 *	0	0	0	0.0 NS
Bone tissue	1 c	2 b	3 a	0.77 *	1 c	3 a	3 a	0.82 *	1 b	3 a	3 a	0.82 *

Means having with the different letters in same row differed significantly. * (P≤0.05), NS: Non-Significant; LSD: least significant difference; 1st: control group; FSH: fish swim bladder; HC: Haversian canal, BMC: bone marrow clot, GT: granulation tissue; BV: blood vessels.

Discussion

Decellularization is a method to obtain ECM from natural-derived tissues or organs by removing cellular components and antigens, by which the immunological danger of transplantation will be eliminated while retaining the three-dimensional structure of the ECM (usually composed of collagen and elastin), glycosaminoglycans (GAGs), and functional proteins (proteoglycans and growth factors) Thus, allogeneic or xenogeneic tissues or organs can be reused for repair and reconstruction after tissue injury (42). Several methods have been utilized to accomplish the decellularization procedure, such as chemical methods with acid (43).

In the present study, the decellularized scaffolds were sterilized with 0.1% Peracetic acid (PAA) and 4% ethanol

solution for 2 hours. Some studies indicated that peracetic acid (PAA) and ethanol are commonly used to sterilize decellularized extracellular matrix (dECM) biomaterials for tissue engineering applications. The combination of PAA and ethanol eliminates bacterial, fungal, and viral contaminations and spores (44-50). On the other hand, (36) said that PAA and ethanol are effective sterilizing agents for dECM scaffolds that preserve the native ECM composition and structure while eliminating cellular material and potential contaminants. The sterilized dECM can then be used for tissue engineering applications.

Bone marrow (BM) is a semi-solid tissue comprising various cell types and is located inside the central cavities of axial and long bones (51). Aspiration of the BM offers an abundant supply of various cellular and molecular components that have different beneficial effects on cartilage, bone, and soft tissue regeneration (48,52).

The histological sections of the bone marrow in the current study revealed a variety of hematopoietic cells, including neutrophils, lymphocytes, megakaryocytes and erythroid cells and considered (53), which classified the cell population found in the bone marrow into two categories: hematopoietic types (monocytes, osteoclasts, megakaryocytes, lymphocytes, and neutrophils) and non-hematopoietic types (osteoblasts, endothelial cells, pericytes, adipocytes, and Schwann cells). Each type of cell is vital in regulating the BM niche.

Neutrophils are essential for the healing of bone fractures. In the first 48 hours following injury, they deposit a fibronectin matrix in the fracture hematoma, contributing to the formation of a fracture hematoma and the early inflammatory response. They also secrete cytokines, such as IL-1, IL-6, IL-10, and TNF-α, which draw monocytes, which later develop into macrophages. When the inflammatory phase progresses, these cytokines also enhance the concentration of pro- and anti-inflammatory substances in the fracture hematoma and eliminate cellular and tissue debris and thrombus. Consequently, their recruitment and function are essential to start the downstream reactions that result in bone regeneration (54).

On the other hand, lymphoid cells (T and B cells) have a critical effect in bone fracture healing, though their effects are still being worked out; immune cells, such as lymphocytes, macrophages, and eosinophils, infiltrate the fracture callus and secrete cytokines that help control the recruitment, proliferation, differentiation, and activation of cells involved in the bone healing process. In particular, T cells seem to regulate the rate at which endochondral bone forms by regulating the osteogenic (bone-forming) cells' mineralization potential. Though the exact processes underlying this are still being worked out, the overall search results showed that lymphoid cells, particularly T cells, have a significant modulatory function in coordinating the various stages of bone fracture repair (55).

The large bone marrow cells known as megakaryocytes (MKs) are responsible for producing platelets and are crucial in controlling bone metabolism and accelerating bone healing. They secrete a high quantity of TGF-β1, which stimulates the growth and differentiation of osteoblasts and angiogenesis, combining the two processes to improve bone formation and the healing of fractures (56). BMA tends to clot when collected because it contains megakaryocytes, platelets, and coagulation factors. Some studies suggested that clot formation may be advantageous while using BMA (32,57). Additionally, there is a compelling biological argument favouring using BMA clots in tissue regeneration techniques. First off, it is not necessary to add any additional items that could interfere with the biological potential. Secondly, platelet degranulation is vital for clot formation and will send several osteotropic cytokines and growth factors to the injury site. Another significant aspect of the creation of clots is that the ensuing fibrinolytic activity may offer an extra supply of angiogenic factors from fibrin breaks, which would be extremely helpful for the engraftment of the cells (58).

Erythroid cells in the bone marrow play a significant role in bone healing and overall bone homeostasis through various mechanisms, primarily influenced by erythropoietin (EPO) and the interactions within the bone marrow microenvironment (59). The bone marrow is a dynamic environment where erythroid cells interact with other cell types, including macrophages and osteoblasts. Macrophages are crucial in maintaining the bone marrow microenvironment and regulating erythropoiesis and bone homeostasis. They support erythroid progenitor differentiation and influence the balance between bone formation and resorption (60).

The histopathological scores in the current study showed a significant increase in active osteoblasts, osteocytes, Haversian canals and mature bone tissue formation at the 4^{th}, 8^{th} and 12^{th} post-operation and a significant increase in osteoclasts at 4^{th} and 8^{th} weeks post operation in both treated groups as compared to control group, this may be attributed to acellular FSB scaffolds that wrapped the segmental bone defect in both treated groups which provide a collagen-rich matrix that supports bone regeneration. Several studies stated that the collagen type I, which is the primary scaffold component, providing a structural framework for new bone formation; they explained that the porous structure and interconnectivity of ECM within the scaffold allows for ingrowth of blood vessels and infiltration of different types of cells including mesenchymal stem cells (MSCs), osteoblasts, and osteoclasts; these cells proliferate and differentiate within the ECM scaffold that participate in bone regeneration (61-63).

On the other hand, stated in their studies on healing large irregular bone defects in rabbit models that the use of small intestinal submucosa (SIS) as a collagen scaffold promotes significant cell infiltration and angiogenesis through

abundant micro-vessel formation and enhanced osteogenesis compared to the control (64,65). They explained that mesenchymal stem cells within the SIS scaffold facilitated the formation of new bone tissue, characterized by more vascularization and collagen deposition, which agreed with the current results.

New vascularization was significantly increased in both treated groups in the present study at 4th and 8th weeks post operation as compared to the control group, and the woven bone originating from the defect edges grows into the scaffold, eventually replacing the ECM material with mature bone tissue at 12th week post operation, this may occur as a result of osteoinductive and osteoconductive properties of ECM scaffolds that lead to new bone formation within the defect site (61-66). Furthermore, ECM scaffolds facilitate and promote the ingrowth of blood vessels, which is essential for supplying necessary nutrients, oxygen, and waste removal during bone regeneration. Establishing a vascular network within the scaffold is critical for successful bone repair (63).

On the other hand, new bone branched was observed to be attached to the FSB membrane remnant at the 8th week post-operation in FSB treated group. This suggests the FSB scaffold is bioresorbable and gradually degrades as new bone forms. According to some authors, the scaffold degradation rate should correspond with the rate of new bone formation to maintain structural integrity and support bone regeneration (67). They added that using ECM scaffolds in bone defects also encourages a favourable histological response, including collagen deposition, cell infiltration and proliferation, osteogenic differentiation, new bone formation, vascularization, and scaffold degradation, ultimately resulting in successful bone regeneration.

The inflammatory responses were significantly observed with mononuclear cells at the 4th and 8th week post-operation in both treated groups and disappeared at the 12th week post-operation. The biodegradation of SIS scaffolds used in their studies modulated the inflammatory response at the implantation site. Although some inflammation is expected at first, over time, it has been seen that the breakdown products of SIS minimize excessive inflammatory reactions, hence improving the environment for bone repair (68).

In FSB-BMC treated group the histopathological scores showed a significant increase in osteoblast, osteocyte, Haversian canals, new vascularization with bone tissue formation at early stage of present study (4th week post operation) and complete bone bridging was observed from week 8 post operation as compared to other two groups, this related to the synergistic effects of FSB scaffold combined with autologous bone marrow clot that trapped reparative cells and active growth factors, as well as the hematoma formed as result of fracture which can enhance the osteogenic potential in bone regeneration process, when SIS scaffold is used in conjunction with other bone-regenerating substances like hydroxyapatite or growth factors, it has a synergistic effect on tissue regeneration, the controlled release of these bioactive agents from gradual degradation of biological scaffolds such as SIS promote cell infiltration, angiogenesis, and inflammation modulation that creating an ideal environment for bone formation and integration (69-71).

Bone marrow aspirate clot (BMA clot) is created by the naturally occurring clotting process of bone marrow aspirate, which contains a rich source of hematopoietic, mesenchymal stem cells (MSCs), growth factors, and cytokines that are essential for bone and cartilage healing by creating an environment that is favorable for cell proliferation and differentiation, making it an important tool in regenerative medicine (72,73). Other researchers have shown that bone marrow clot (BMC) is a biological scaffold and a source of regenerative cells that preserve all the essential components of the aspirated bone marrow required for healing. These components include platelets that release growth factors like bone morphogenetic proteins (BMPs) and platelet-derived growth factor (PDGF), as well as a matrix that is vital for promoting angiogenesis, differentiation, and cell proliferation, all of which are necessary for a successful bone healing process. It has been shown to have similarities to fracture hematoma, which is essential for bone remodeling and healing (32,73,74).

In the FSB-BMC treated group at week 8 post-operation, a complete replacement of the fracture site with thick lamellar bone lining with active osteoblast was observed. The compact bone was filled at the defect site and fused with the host old bone edges at week 12 post-operation. The therapeutic potentials of autologous bone graft (ABG) and autologous bone marrow aspirate (29). They hypothesized that coagulated BMA is as successful as an autologous bone graft in repairing long bone defects (75). They noted that the BMA healing process does not involve the resorption of bone graft fragments that may prolong the reparative cascade, supporting the idea that therapeutic efficacy in bone healing depends largely on osteogenic cells and osteoinductive growth factors, which are present in both autograft and BMA.

The histopathological scores in the control group in the current study showed a significant decrease in osteoblast, osteocytes, mature bone, Haversian canals and bone tissue formation at intervals 4, 8, and12 weeks post-operation, indicating poor bone healing as compared to both treated groups. More fibrous tissue appeared in the center of the defect area at both 4- and 8-weeks post-operation compared to treated groups. The sections in the control group in the fourth-week post-operation showed small amounts of new bone tissue widely spaced by vascular fibrous tissue attached to the host bone from the periphery with patches of cartilage formation at the host bone edges (76).

The new cartilage formation in the defect accompanied the formation of new bone, indicating endochondral ossification and mineralized woven bone; these findings

further support the favorable osteogenic potential of cartilage (77). Consequently, the existence of cartilage within the defect is a crucial indicator of osteogenesis taking place during the soft callus phase, during which proliferating cartilage's matrix mineralization converts soft callus into hard callus (78,79); in contrast to newly formed cartilage, the presence of fibrous tissue indicates low osteogenic activity. When newly formed fibrous tissue coexists with newly formed bone, no transition exists between the fibrous tissue and newly formed bone, and excessive fibrous tissue production is recognized as an essential factor in bone non-union (80). At 12 weeks post-operation, the sections showed irregular delicate trabecular bone with a moderate amount of lamellar bone formation with irregular bone tissue, and the trabecular bone formation decreased toward the defective center (81).

Conclusions

This study demonstrates that FSB scaffolds, especially when combined with autologous BMA clots, significantly enhance bone regeneration in rabbits with radial bone defects. The FSB scaffolds provided a collagen-rich matrix that supported cell infiltration, vascularization, and osteogenesis, with the FSB-BMC group showing the highest levels of osteoblast activity and bone formation. These results suggest that FSB combined with BMA clot offers a promising alternative to traditional bone repair graft, highlighting its potential applications in regenerative medicine. Further studies could explore scaffold optimization and long-term outcomes.

Acknowledgements

The authors thank the members of the surgery department at the University of Baghdad's College of Veterinary Medicine for their help with this work.

Conflict of interest

The authors of this article worked on it and declared that they had no conflicts of interest.

References

1. Qu H, Fu H, Han Z, Sun Y. Biomaterials for bone tissue engineering scaffolds: A review. RSC Adv. 2019;9:26252-62. DOI: 10.1039/C9RA05214C
2. Pereira HF, Cengiz IF, Silva FS, Reis RL, Oliveira JM. Scaffolds and coatings for bone regeneration. J Mater Sci Mater Med. 2020;31:27. DOI: 10.1007/s10856-020-06364-y
3. Huang Q, Liu Y, Ouyang Z, Feng Q. Comparing the regeneration potential between PLLA/Aragonite and PLLA/Vaterite pearl composite scaffolds in rabbit radius segmental bone defects. Bioact Mater. 2020;5(4):980-9. DOI: 10.1016/j.bioactmat.2020.06.018
4. Atiyah AG, AL-Falahi NR, Hasan MS, Owain MS. Study the effect of avian eggshell hydroxyapatite powder on bone gaps healing in rabbits. Vet Pract. 2020;21(1):429-34. [available at]
5. Jonitz A, Lochner K, Lindner T, Hansmann D, Marrot A, Bader R. Oxygen consumption, acidification and migration capacity of human primary osteoblasts within a three-dimensional tantalum scaffold. J Mater Sci Mater Med. 2011;22:2089-95. DOI: 10.1007/s10856-011-4384-6
6. Mollon B, Kandel R, Chahal J, Theodoropoulos J. The clinical status of cartilage tissue regeneration in humans. Osteoarthritis Cartilage. 2013;21(12):1824-33. DOI: 10.1016/j.joca.2013.08.024
7. Turnbull G, Clarke J, Picard F, Riches P, Jia L, Han F, Shu W. 3D bioactive composite scaffolds for bone tissue engineering. Bioact Mater. 2018;3(3):278-314. DOI: 10.1016/j.bioactmat.2017.10.001
8. Wubneh A, Tsekoura EK, Ayranci C, Uludağ H. Current state of fabrication technologies and materials for bone tissue engineering. Acta Biomater. 2018;80:1-30. DOI: 10.1016/j.actbio.2018.09.031
9. Peric M, Dumic-Cule I, Grcevic D, Matijasic M, Verbanac D, Paul R, Grgurevic L, Trkulja V, Bagi CM, Vukicevic S. The rational use of animal models in the evaluation of novel bone regenerative therapies. Bone. 2015;70:73-86. DOI: 10.1016/j.bone.2014.07.010
10. Al-Falahi NH. Comparative study for using of submucosa of small intestine in healing of clean and infected avulsion wounds. Iraqi J Vet Med. 2009;33(1):90-7. DOI: 10.30539/iraqijvm.v33i1.720
11. AL-Falahi NH, Salih SI, Obaid AH. A comparative biomechanical study of repaired tendons wrapped with two biological matrices in bucks. Iraqi J Vet Med. 2016;40(1):73-8. DOI: 10.30539/iraqijvm.v40i1.141
12. Al-Bayati AH, Al-Tememe HA, Al-Mudallal NH. Role of acellular bovine urinary bladder submucosa on skin wound healing in Iraqi goats. Iraqi J Vet Med. 2016;40(1):53-60. DOI: 10.30539/iraqijvm.v40i1.138
13. Al-Falahi NH, Ab Abood D, Dauood MS. Comparative evaluation of bovine pericardial membrane and amniotic membrane in wounds skin healing in rabbits. Iraqi J Vet Med. 2017;41(2):137-45. DOI: 10.30539/iraqijvm.v41i2.63
14. Al-Ebadi AK, Al-Bayati AH. Effect of acellular bovine pericardium and urinary bladder submucosa matrixes in reconstruction of ventrolateral hernias in bucks; molecular evaluation. Iraqi J Vet Med. 2019;43(1):67-74. DOI: 10.30539/iraqijvm.v43i1.474
15. Gumaa BH, Al-Bayati AH. Molecular evaluation of efficacy of freshwater and marine acellular fish skin matrixes in reconstruction of ventrolateral hernia in bucks. Indian J Forensic Med Toxicol. 2021;15(4):880-6. DOI: 10.37506/ijfmt.v15i4.16814
16. Mohammed MS, Salih SI. Histopathological Study of Using Fetal Caprine Acellular Dermal Matrix Alone and in Combination with Non-thermal Plasma in Healing of Full-thickness Acute Skin Wounds in Bucks. Int J Health Sci. 2022;6(3):8784-806. DOI: 10.53730/ijhs.v6nS3.8105
17. Mohammad FA, Al-Ebadi AK. Macroscopic and histopathological study of using fenestrated and non-fenestrated catfish acellular dermal matrix on healing ventro-lateral hernia in bucks. J Surv Fish Sci. 2023;10(3S):844-59. DOI: 10.17762/sfs.v10i3S.91
18. Badylak SF. The extracellular matrix as a biological scaffold material. Biomaterials. 2007;28(25):3587-93. DOI: 10.1016/j.biomaterials.2007.04.043
19. Saiegh AM, Al-Hyani OH, Alheyali KW. Using lyophilized bovine pericardium and acellular ovine esophageal mucosa to repair cerebral dura mater defect in dogs. Iraqi J Vet Sci. 2024;38(2):379-389. DOI: 10.33899/ijvs.2023.142111.3159
20. Zaki MM, Ibrahim SM, Ibrahim MM. Comparison between acellular ovine skin and acellular bovine pericardium on the induced skin loss healing in local breed cats. Iraqi J Vet Sci. 2024;38(4):949-961. DOI: 10.33899/ijvs.2024.151344.3750
21. Al-Hyani OH, Ibrahim SM, Al-Saiegh AM. Evaluation of the efficacy of freeze-dried bovine pericardium and acellular bovine skin in the treatment of diaphragmatic hernia in dogs. Iraqi J Vet Sci. 2024;38(2):411-9. DOI: 10.33899/ijvs.2023.142649.3189
22. Mredha MT, Kitamura N, Nonoyama T, Wada S, Goto K, Zhang X, Nakajima T, Kurokawa T, Takagi Y, Yasuda K, Gong JP. Anisotropic tough double network hydrogel from fish collagen and its spontaneous in vivo bonding to bone. Biomaterials. 2017;132:85-95. DOI: 10.1016/j.biomaterials.2017.04.005

23. Bai H, Sun P, Wu H, Wei S, Xie B, Wang W, Hou Y, Li JA, Dardik A, Li Z. The application of tissue-engineered fish swim bladder vascular graft. Commun Biol. 2021;4(1):1153. DOI: 10.1038/s42003-021-02696-9
24. Luan Z, Liu S, Wang W, Xu K, Ye S, Dan R, Zhang H, Shu Z, Wang T, Fan C, Xing M. Aligned nanofibrous collagen membranes from fish swim bladder as a tough and acid-resistant suture for pH-regulated stomach perforation and tendon rupture. Biomater Res. 2022;26(1):60. DOI: 10.1186/s40824-022-00306-1
25. Veronesi F, Giavaresi G, Tschon M, Borsari V, Nicoli Aldini N, Fini M. Clinical use of bone marrow, bone marrow concentrate, and expanded bone marrow mesenchymal stem cells in cartilage disease. Stem Cells Dev. 2013;22(2):181-92. DOI: 10.1089/scd.2012.0373
26. Fortier LA, Potter HG, Rickey EJ, Schnabel LV, Foo LF, Chong LR, Stokol T, Cheetham J, Nixon AJ. Concentrated bone marrow aspirate improves full-thickness cartilage repair compared with microfracture in the equine model. J Bone Joint Surg Am. 2010;92(10):1927-37. DOI: 10.2106/JBJS.I.01284
27. Gangji V, De Maertelaer V, Hauzeur JP. Autologous bone marrow cell implantation in the treatment of non-traumatic osteonecrosis of the femoral head: Five-year follow-up of a prospective controlled study. Bone. 2011;49(5):1005-9. DOI: 10.1016/j.bone.2011.07.032
28. Veronesi F, Salamanna F, Tschon M, Maglio M, Nicoli Aldini N, Fini M. Mesenchymal stem cells for tendon healing: What is on the horizon. J Tissue Eng Regen Med. 2017;11(11):3202-19. DOI: 10.1002/term.2209
29. Lim ZX, Rai B, Tan TC, Ramruttun AK, Hui JH, Nurcombe V, Teoh SH, Cool SM. Autologous bone marrow clot as an alternative to autograft for bone defect healing. Bone Joint Res. 2019;8(3):107-17. DOI: 10.1302/2046-3758.83.BJR-2018-0096.R1
30. Thanoon M, Eesa MJ, Abed ER. Effects of platelets rich fibrin and bone marrow on the healing of distal radial fracture in local dogs: Comparative study. Iraqi J Vet Sci. 2019;33(2):419-25. DOI: 10.33899/ijvs.2019.163169
31. Eesa MJ, Thanoon MG, Ibrahim SM. The Effect of bone marrow autograft on fracture healing with destruction of periosteum and endosteum in rabbits. Iraqi J Vet Sci. 2006;20(2):163-72. DOI: 10.33899/ijvs.2006.62494
32. Salamanna F, Contartese D, Nicoli Aldini N, Barbanti Brodano G, Griffoni C, Gasbarrini A, Fini M. Bone marrow aspirate clot: A technical complication or a smart approach for musculoskeletal tissue regeneration. J Cell Physiol. 2018;233(4):2723-32. DOI: 10.1002/jcp.26065
33. Sivajothi S, Reddy SB, Rayulu VC. Effect of Ivermectin against Psoroptic mange in rabbits. Int J Sci World. 2014;2(1):10-2. DOI: 10.14419/ijsw.v2i1.1893
34. Crapo PM, Gilbert TW, Badylak SF. An overview of tissue and whole organ decellularization processes. Biomaterials. 2011;32(12):3233-43. DOI: 10.1016/j.biomaterials.2011.01.057
35. Kumar V, Kumar N, Gangwar AK, Singh H, Singh R. Comparative histologic and immunologic evaluation of 1, 4-butanediol diglycidyl ether crosslinked versus non-crosslinked acellular swim bladder matrix for healing of full-thickness skin wounds in rabbits. J Surg Res. 2015;197(2):436-46. DOI: 10.1016/j.jss.2015.04.080
36. Tao M, Ao T, Mao X, Yan X, Javed R, Hou W, Wang Y, Sun C, Lin S, Yu T. Sterilization and disinfection methods for decellularized matrix materials: Review, consideration, and proposal. Bioact Mater. 2021;6(9):2927-45. DOI: 10.1016/j.bioactmat.2021.02.010
37. Flecknell P. Laboratory animal anaesthesia. 4th ed. USA: Academic Press; 2015. 220-2 p.
38. Al-Haideri DH, Al-Timmemi HA. Efficacy of chitosan nanoparticles and mesenchymal stem cells in rabbit models for sciatic nerve regeneration. Iraqi J Vet Sci. 2024;38(2):369- 377. DOI: 10.33899/ijvs.2023.142572.3186
39. Awid AC, Alfaris AA, Sawad AA. Effects of the cyclosporine on some hematological indices in bone marrow transplanted rabbits. Basrah J Vet Res. 2014;1(2):23-35. DOI: 10.33762/bvetr.2014.98790
40. Ahmad A, Nawaz R, Soomro SA, Rao N, Qasim M. The effects of meloxicam, a non-steroidal anti-inflammatory drug, on the biochemical parameters of rabbits. Int J Biosci. 2017;11(2):58-67. DOI: 10.12692/ijb/11.2.58-67
41. Bigham-Sadegh A, Torkestani HS, Sharifi S, Shirian S. Effects of concurrent use of royal jelly with hydroxyapatite on bone healing in rabbit model: Radiological and histopathological evaluation. Heliyon. 2020;6(7):e04547. DOI: 10.1016/j.heliyon.2020.e04547
42. Lan X, Luo M, Li M, Mu L, Li G, Chen G, He Z, Xiao J. Swim bladder-derived biomaterials: structures, compositions, properties, modifications, and biomedical applications. J Nanobiotechnol. 2024;22(1):186. DOI: 10.1186/s12951-024-02449-w
43. Gilbert TW, Wognum S, Joyce EM, Freytes DO, Sacks MS, Badylak SF. Collagen fibre alignment and biaxial mechanical behaviour of porcine urinary bladder derived extracellular matrix. Biomaterials. 2008;29(36):4775-82. DOI: 10.1016/j.biomaterials.2008.08.022
44. Poornejad N, Nielsen JJ, Morris RJ, Gassman JR, Reynolds PR, Roeder BL, Cook AD. Comparison of four decontamination treatments on porcine renal decellularized extracellular matrix structure, composition, and support of renal tubular epithelium cells. J Biomater Appl. 2016;30(8):1154-67. DOI: 10.1177/0885328215615760
45. Balestrini JL, Liu A, Gard AL, Huie J, Blatt KM, Schwan J, Zhao L, Broekelmann TJ, Mecham RP, Wilcox EC, Niklason LE. Sterilization of lung matrices by supercritical carbon dioxide. Tissue Eng Part C Methods. 2016;22(3):260-9. DOI: 10.1089/ten.tec.2015.0449
46. Dai Z, Ronholm J, Tian Y, Sethi B, Cao X. Sterilization techniques for biodegradable scaffolds in tissue engineering applications. J Tissue Eng. 2016;7:2041731416648810. DOI: 10.1177/2041731416648810
47. Poornejad N. Decellularization and recellularization processes for whole porcine kidneys [Ph.D. dissertation]. USA: Brigham Young University; 2017.
48. Farooq AA, Khan MA, Akbar HA, Hayat MA, Murtaza SM, Shah MH, Javid MA, Saleem MU, Abdul Basit MA, Inayat SI, Lashari MH. Effects of autologous bone marrow on the healing of long bones fractures reduced by external skeletal fixators in goats. Iraqi J Vet Sci. 2023;37(4):963-969. DOI: 10.33899/ijvs.2023.137990.2759
49. Zhang X, Chen X, Hong H, Hu R, Liu J, Liu C. Decellularized extracellular matrix scaffolds: Recent trends and emerging strategies in tissue engineering. Bioact Mater. 2022;10:15-31. DOI: 10.1016/j.bioactmat.2021.09.014
50. Shyam R, Palaniappan A. Effect of sterilization techniques on biomaterial inks' properties and 3D bioprinting parameters. Bioprint. 2023;e00294. DOI: 10.1016/j.bprint.2023.e00294
51. Kumar R, Godavarthy PS, Krause DS. The bone marrow microenvironment in health and disease at a glance. J Cell Sci. 2018;131(4):jcs201707. DOI: 10.1242/jcs.201707
52. Radcliffe CH, Flaminio MB, Fortier LA. Temporal analysis of equine bone marrow aspirate during establishment of putative mesenchymal progenitor cell populations. Stem Cells Dev. 2010;19(2):269-82. DOI: 10.1089/scd.2009.0091
53. Birbrair A, Frenette PS. Niche heterogeneity in the bone marrow. Ann N Y Acad Sci. 2016;1370(1):82-96. DOI: 10.1111/nyas.13016
54. Kovtun A, Bergdolt S, Wiegner R, Radermacher P, Huber-Lang M, Ignatius A. The crucial role of neutrophil granulocytes in bone fracture healing. Eur Cell Mater. 2016;32:152-62. DOI: 10.22203/eCM.v032a10
55. Baht GS, Vi L, Alman BA. The role of the immune cells in fracture healing. Curr Osteoporos Rep. 2018;16:138-45. DOI: 10.1007/s11914-018-0423-2
56. Tang Y, Hu M, Xu Y, Chen F, Chen S, Chen M, Qi Y, Shen M, Wang C, Lu Y, Zhang Z. Megakaryocytes promote bone formation through coupling osteogenesis with angiogenesis by secreting TGF-β1. Theranostics. 2020;10(5):2229-42. DOI: 10.7150/thno.40559
57. Malara A, Abbonante V, Di Buduo CA, Tozzi L, Currao M, Balduini A. The secret life of a megakaryocyte: Emerging roles in bone marrow homeostasis control. Cell Mol Life Sci. 2015;72:1517-36. DOI: 10.1007/s00018-014-1813-y
58. Palta S, Saroa R, Palta A. Overview of the coagulation system. Indian J Anaesth. 2014;58(5):515-23. DOI: 10.4103/0019-5049.144643

59. Suresh S, Lee J, Noguchi CT. Effects of erythropoietin in white adipose tissue and bone microenvironment. Front Cell Dev Biol. 2020;8:584696. DOI: 10.3389/fcell.2020.584696
60. Arcasoy MO. Non-erythroid effects of erythropoietin. Haematol. 2010;95(11):1803. DOI: 10.3324/haematol.2010.030213
61. Lin X, Patil S, Gao YG, Qian A. The bone extracellular matrix in bone formation and regeneration. Front Pharmacol. 2020;11:757. DOI: 10.3389/fphar.2020.00757
62. Filippi M, Born G, Chaaban M, Scherberich A. Natural polymeric scaffolds in bone regeneration. Front Bioeng Biotechnol. 2020;8:474. DOI: 10.3389/fbioe.2020.00474
63. Amirazad H, Dadashpour M, Zarghami N. Application of decellularized bone matrix as a bioscaffold in bone tissue engineering. J Biol Eng. 2022;16(1):1. DOI: 10.1186/s13036-021-00282-5
64. Zhao L, Zhao J, Yu JJ, Zhang C. Irregular bone defect repair using tissue-engineered periosteum in a rabbit model. Tissue Eng Regen Med. 2020;17:717-27. DOI: 10.1007/s13770-020-00282-4
65. Xiao H, Chen X, Liu X, Wen G, Yu Y. Recent advances in decellularized biomaterials for wound healing. Mater Today Bio. 2023;19:100589. DOI: 10.1016/j.mtbio.2023.100589
66. Taguchi Y, Amizuka N, Nakadate M, Ohnishi H, Fujii N, Oda K, Nomura S, Maeda T. A histological evaluation for guided bone regeneration induced by a collagenous membrane. Biomaterials. 2005;26(31):6158-66. DOI: 10.1016/j.biomaterials.2005.03.023
67. Finze R, Laubach M, Russo Serafini M, Kneser U, Medeiros Savi F. Histological and immunohistochemical characterization of osteoimmunological processes in scaffold-guided bone regeneration in an ovine large segmental defect model. Biomedicines. 2023;11(10):2781. DOI: 10.3390/biomedicines11102781
68. Yeung DA, Kelly NH. The role of collagen-based biomaterials in chronic wound healing and sports medicine applications. Bioengineering. 2021;8(1):8. DOI: 10.3390/bioengineering8010008
69. Zhao Y, Peng H, Sun L, Tong J, Cui C, Bai Z, Yan J, Qin D, Liu Y, Wang J, Wu X. The application of small intestinal submucosa in tissue regeneration. Mater Today Bio. 2024;101032. DOI: 10.1016/j.mtbio.2024.101032
70. Casarin M, Fortunato TM, Imran S, Todesco M, Sandrin D, Borile G, Toniolo I, Marchesan M, Gerosa G, Bagno A, Romanato F. Porcine small intestinal submucosa (SIS) as a suitable scaffold for the creation of a tissue-engineered urinary conduit: Decellularization, biomechanical and biocompatibility characterization using new approaches. Int J Mol Sci. 2022;23(5):2826. DOI: 10.3390/ijms23052826
71. Lana JF, da Fonseca LF, Mosaner T, Tieppo CE, Azzini GO, Ribeiro LL, Setti T, Purita J. Bone marrow aspirate clot: A feasible orthobiologic. J Clin Orthop Trauma. 2020;11:S789-94. DOI: 10.1016/j.jcot.2020.07.003
72. Salamanna F, Tedesco G, Sartori M, Griffoni C, Spinnato P, Romeo P, et al. Safety and efficacy of autologous bone marrow clot as a multifunctional bioscaffold for instrumental posterior lumbar fusion: A 1-year follow-up pilot study. Front Endocrinol. 2024;14:1245344. DOI: 10.3389/fendo.2023.1245344
73. Salamanna F, Contartese D, Borsari V, Pagani S, Barbanti Brodano G, Griffoni C, Ricci A, Gasbarrini A, Fini M. Two hits for bone regeneration in aged patients: Vertebral bone marrow clot as a biological scaffold and powerful source of mesenchymal stem cells. Front Bioeng Biotechnol. 2022;9:807679. DOI: 10.3389/fbioe.2021.807679
74. Krzymanski G, Kalczak M, Wiktor-Jedrzejczak W. The use of bone-marrow-derived fibroblastoid cells and fresh bone marrow in the treatment of bone defects: An experimental study. Int J Oral Maxillofac Surg. 1997;26:55-60. DOI: 10.1016/S0901-5027(97)80850-8
75. Li J, Wang W, Li M, Liu L. Repair of segmental bone defect using tissue engineered heterogeneous deproteinized bone doped with lithium. Sci Rep. 2021;11(1):4819. DOI: 10.1038/s41598-021-84526-w
76. Vasques AM, Bueno CR, Guimarães MR, Valentim D, da Silva AC, Benetti F, Santos JM, Cintra LT, Dezan Junior E. Histological bone-healing evaluation of critical-size defects filled with β-tricalcium phosphate in rat tibiae. Appl Sci. 2024;14(9):3821. DOI: 10.3390/app14093821
77. Yang L, Tsang KY, Tang HC, Chan D, Cheah KS. Hypertrophic chondrocytes can become osteoblasts and osteocytes in endochondral bone formation. Proc Natl Acad Sci U S A. 2014;111(33):12097-102. DOI: 10.1073/pnas.1302703111
78. Gredes T, Wróbel-Kwiatkowska M, Dominiak M, Gedrange T, Kunert-Keil C. Osteogenic capacity of transgenic flax scaffolds. Biomed Eng. 2012;57(1):53-58. DOI: 10.1515/bmt-2011-0035
79. Schell H, Duda GN, Peters A, Tsitsilonis S, Johnson KA, Schmidt-Bleek K. The hematoma and its role in bone healing. J Exp Orthop. 2017;4(1):5. DOI: 10.1186/s40634-017-0079-3
80. Pabbruwe MB, Standard OC, Sorrell CC, Howlett CR. Bone formation within alumina tubes: Effect of calcium, manganese, and chromium dopants. Biomaterials. 2004;25(20):4901-10. DOI: 10.1016/j.biomaterials.2004.01.005
81. Zhao MD, Huang JS, Zhang XC, Gui KK, Xiong M, Yin WP, Yuan FL, Cai GP. Construction of radial defect models in rabbits to determine the critical size defects. PLoS One. 2016;11(1):e0146301. DOI: 10.1371/journal.pone.0146301

إعادة بناء عيب عظم الكعبرة المحدث تجريبيا في الأرانب باستخدام مثانة سباحة الأسماك اللاخلوية وخثرة نخاع العظم الذاتي: تقييم نسجي مرضي

نور الهدى احمد مهدي و نادية حميد رجه مهدي

فرع الجراحة والتوليد، كلية الطب البيطري، جامعة بغداد، بغداد، العراق

الخلاصة

في الدراسة الحالية تم استخدام خمس وأربعون أرنبا بالغا سليما سريريا، تراوح متوسط أعمارهم بين ٩-١٢ شهرا، و بأوزان ١,٥-١,٧ كغم وتم تقسيمهم عشوائيا إلى ثلاث مجموعات متساوية (العدد=١٥)، في جميع الحيوانات تم إنشاء قطع عظمي بمقدار ٥ ملم في منتصف عمد عظم الكعبرة، في مجموعة السيطرة (العدد=١٥) ترك القطع العظمي دون أي إضافات، في المجموعة المعالجة بمثانة السباحة للأسماك (المجموعة الثانية) تم لف العيوب المحدثة باستخدام مثانة السباحة منزوعة الخلايا المعدة مسبقا وتم خياطته حول القطع العظمي، في مجموعة المعالجة بمثانة السباحة للأسماك مع خثرة نخاع العظم الذاتي (المجموعة الثالثة) تم لف العيوب التي تم إحداثها باستخدام مثانة السباحة للأسماك كما هو موضح سابقا بعد ملئ القطع العظمي بخثرة نخاع العظم الذاتي. تم تقييم العيوب القطعية في جميع المجموعات نسجيا مرضيا في الأسابيع ٤ و ٨ و ١٢ بعد العملية لمراقبة تكوين العظام وجسر عيوب العظام القطعية. أظهرت النتائج زيادة كبيرة في الخلايا العظمية وقنوات هافرس والأوعية الدموية الجديدة وتكوين النسيج العظمي في المجموعة الثالثة مقارنة بالمجموعات الأخرى في ٤ أسابيع بعد العملية. في ٨ و١٢ أسبوعا بعد الجراحة، أظهرت كلتا المجموعتين المعالجتين زيادة كبيرة في الخلايا العظمية والعظام الناضجة وعوارض العظام وقنوات هافرس النسيج العظمي مقارنة بمجموعة السيطرة. في الاستنتاج، أظهرت المجموعة الثالثة تكوينا عظميا جديدا أعلى وجسرا كاملا مقارنة بالمجموعات الأخرى، بينما أظهرت المجموعة الثانية تكوينا عظميا جديدا وجسرا جزئيا مقارنة بمجموعة السيطرة.